Dust Dynamics in the Rings of Chariklo

by

Juliet A. Pilewskie

Bachelor of Arts – Department of Physics

Undergraduate Honors Thesis

Defense Copy

Thesis defense committee:

Mihály Horányi	Advisor	Department of Physics
Tobin Munsat	Honors Council Representative	Department of Physics
Robert Anderson	Outside Representative	Department of Geological Sciences

Defended:

April 5$^{\text{th}}$, 2017

This thesis entitled:
Dust Dynamics in the Rings of Chariklo
written by Juliet A. Pilewskie
has been approved for the Department of Physics

_____

Prof. Mihály Horányi

_____

Prof. Tobin Munsat

_____

Prof. Robert Anderson

Date _____

The final copy of this thesis has been examined by the signatories, and we find that both the content and the form meet acceptable presentation standards of scholarly work in the above mentioned discipline.

Pilewskie, Juliet A. (B.A., Physics)

Dust Dynamics in the Rings of Chariklo

Thesis directed by Prof. Mihály Horányi

Two years ago, the centaur Chariklo was discovered to have two rings, which made it the first known minor planet to have a ring system. The uniqueness of this situation calls for an examination as to how a two-ring system can be sustained around a relatively small interplanetary object. We simulate, in 2D and 3D, a two-body system with solar radiation pressure forces perturbing a dust particle's orbit around a Chariklo-sized object. The lifetime of orbiting dust particles is estimated by integrating their orbits as a function of their size and initial position. Current results show that for a water-ice or silicate particle with radius of $100\,\mu m$, its simulated orbit lasts for only about 20 years. This short lifetime suggests that there may be additional forces keeping the ring particle in place, and/or the presence of active sources of these particles. It is also found that the dust particle's simulated orbital lifetime is longest when it is positioned where Chariklo's rings are located, which agrees with the observations already made of Chariklo's ring system. This research is the first step in better understanding the formation and sustainability of non-planetary ring systems.

Dedication

I dedicate this thesis to my family: Peter, Katherine, and Monica Pilewskie, for their continual support and encouragement. Also, I dedicate this thesis to the researchers studying rings around celestial bodies in the hopes that the contents of this thesis are somewhat useful.

Acknowledgements

I would first like to thank Prof. Mihaly Horanyi for hiring me at the Institute for Modeling Plasma, Atmospheres and Cosmic Dust (IMPACT) at LASP and for providing me with incredible opportunities. Also, I would like to thank him for encouraging me and teaching me so much about dust dynamics in rings. I am also very grateful for Sean Hsu's help in debugging several parts of my code, as well as his help in creating the radial distribution plots. Lastly, thanks go to everyone at IMPACT for always being so eager to discuss my research with me. Their input has impacted my research greatly.

Contents

Chapter

Figures

Figure

Chapter 1

Introduction

Planetary dust rings have long been studied since the first detection of Saturn's ring system over 400 years ago. Understanding the dynamics of rings is significant in that they give insight on the formation of planetary systems and galaxies, and the evolution of the objects they orbit. Rings have exclusively been found orbiting the four gas giants of our Solar System until the detection of two rings around the centaur 10199 Chariklo. While there is observational evidence supporting rings around Chariklo, it seems unlikely that Chariklo is capable of maintaining a ring system due to its weak gravitational field and highly eccentric orbit. The focus of my research is to explore the dust dynamics and sustainability of Chariklo's newly discovered rings.

Centaurs are minor planets that have perihelion beyond the orbit of Jupiter and semi-major axes between the outer planets [*Horner et al.*, 2004; *Hyodo et al.*, 2016]. They are named after the mythological centaurs that have mixed features of human and horse because they exhibit mixed properties of asteroids and comets. Some centaurs that are red in color can be classified as asteroids as they most likely have an organic surface layer and a rocky interior. Others exhibit comet-like properties because they can be dark blue-grey with an icy nucleus covered by dust. Most centaurs are not protected by orbital resonances, meaning that a centaur does not have a mutual gravitational attraction with another object to maintain an orbit lasting longer than $10^6 - 10^7$ years [*Delsanti and Jewitt*, 2006].

Chariklo is the largest of the known centaurs with a radius of 124 ± 9 km and a short lifetime of ~ 10 Myr [*Horner et al.*, 2004]. Its dark surface indicates that it might have originated in the

Kuiper belt and drifted into the Solar System less than 10 Mya due to gravitational effects by Uranus. Chariklo is currently located between Saturn and Uranus and has an orbital eccentricity of 0.175 (small for centaurs), semi-major axis of 15.8 AU, and orbital period of 62.74 yr [*Braga-Ribas et al.*, 2014]. Its rotation period is ~ 7 hours [*Fornasier et al.*, 2014].

Chariklo's rings were discovered in 2013. Its ring system comprises two dense rings with orbital radii of 391 km, or $3.15R_0$ where R_0 is Chariklo's radius, and 405 km ($3.26R_0$) and orbital periods of approximately 0.75 days. The present orientation of the rings is consistent with an edge-on geometry measured in 2008, and it corresponds to the apparent dimming of Chariklo's system between 1997-2008 [*Belskaya et al.*, 2010]. During this period there was a gradual disappearance in ice and other absorption materials in Chariklo's spectrum, implying that the rings consist partly of water-ice [*Braga-Ribas et al.*, 2014].

The rings should disperse over a period of, at most, a few million years due to interparticle collisions and Poynting-Robertson drag. Therefore, either the rings are very young or are being actively contained due to external objects such as satellites (shepherd moons). Approximately 5% of centaurs and trans-Neptunian objects have satellites that most likely resulted from three-body captures, impacts, or rotational disruptions. There has not been any clear detection of satellites around Chariklo. If the rings formed while Chariklo was trans-Neptunian nearly 10 Mya [*Braga-Ribas et al.*, 2014], the hypothesis that the rings are being actively confined is supported.

In order to understand the dust dynamics of Chariklo's ring system, I present in the next chapter a background on Chariklo's rings including how they were detected, possible origins, perturbing forces that may be shortening their lifetimes, and the effects that shepherd moons would have on them. The third chapter presents a 2D two-body model in which Chariklo and a single dust particle reside in the xy-plane with the gravitational force from Chariklo and solar radiation pressure force acting on the dust particle in the x-direction. The fourth chapter presents a 3D model with the Sun's radiation pressure included in the z-component of the equations of motion. The final chapter is a discussion of my results.

Chapter 2

Overview of Chariklo's Rings

2.1   Origin of the Rings

While there is no clear understanding as to how Chariklo's rings formed, several hypotheses for their origin have been proposed. All proposed origins consider a debris disk in which the largest fragments act as shepherds for the smaller particles. One possibility is that an impactor hit Chariklo and created the debris disk by removing icy material from Chariklo's outer layers, which would account for the appearance of water-ice in the rings. Or the impactor could have destroyed a pre-existing satellite or was itself disrupted during the impact and its remnants formed the disk. Chariklo has a low escape velocity ($\sim$ 0.1 km s^{-1}), so the only way an impactor could have formed a ring system is if the object impacted at low velocity [*Braga-Ribas et al.*, 2014].

Another possible origin is that a debris disk formed from a rotational disruption of Chariklo or was supplied by cometary-like activity [*Braga-Ribas et al.*, 2014]. Upon arrival into the inner solar system, Chariklo can exhibit cometary activity as it adjusts to new thermal conditions. It only takes a few orbits for the surface to adjust to a new thermal equilibrium, and an external energy source, such as an impactor, would be needed for Chariklo to exhibit any further cometary activity [*Duffard et al.*, 2014; *Guilbert-Lepoutre*, 2011]. It may be more likely that Chariklo's ring system formed from two pre-existing satellites that collided to form a debris disk [*Braga-Ribas et al.*, 2014].

Lastly, the rings could have been created by an extremely close encounter with one of the giant planets [*Hyodo et al.*, 2016]. Since Chariklo's orbit is controlled by Uranus [*Braga-Ribas et al.*, 2014], an encounter with Uranus could have created the rings. In order for the ring system

to form around Chariklo during a close encounter, the centaur needs to pass within the planet's Roche limit, so within 5 Uranus radii. During the close encounter, the icy mantle of the passing object is excavated by the planet's tidal force and the debris forms a disk around the passing object [*Hyodo et al.*, 2016]. The likelihood of Chariklo passing within Uranus' Roche limit is 0.001%, which supports the model of the rings having formed while Chariklo was trans-Neptunian (nearly 10 Mya), and surviving the transition into the Solar System [*Braga-Ribas et al.*, 2014].

2.2   Stellar Occultation

The nature of celestial objects can be studied through events known as occultations in which one object is hidden by another object that passes between it and the observer. On June 3, 2013, Chariklo's system occulted, or blocked from view, an $R = 12.4$ mag star. This event was recorded at three sites in Chile. Seven other sites in Brazil, Argentina, and Uruguay detected a total of thirteen drops in stellar flux known as secondary events. The primary event was the stellar flux interruption from Chariklo. The secondary events provided a measure of the integrated light loss, which determined the occultation's geometry. All of the events produced a geometry consistent with a ring system, as opposed to other interpretations such as an ensemble of cometary jets that can be common among other centaurs [*Braga-Ribas et al.*, 2014].

Fig. 2.1 shows two secondary events resolved by the Danish 1.54-m telescope at the European Southern Observatory at La Silla, Chile. The normalized fluxes depict the intensity of light visible to the observer, and can be used to determine the rings' widths and optical depths. The rings are modeled as sharp-edged, semi-transparent bands of transmission T along the line of sight and apparent width W_{app} along the occultation chord. Optical depth, τ, is related to the fraction of incident light blocked by the ring when it lies between the source and the observer. It is used to quantify ring opacity and is a dimensionless quantity defined by the equation $T = \exp(-2\tau)$ [*Braga-Ribas et al.*, 2014]. The factor of 2 is due to the efficiency of particle extinction Q_e that approaches 2 if the particles are much larger than the wavelength of visible light [*Cuzzi*, 1985].

It was found that at ingress (before the main Chariklo occultation) C1R and C2R have widths
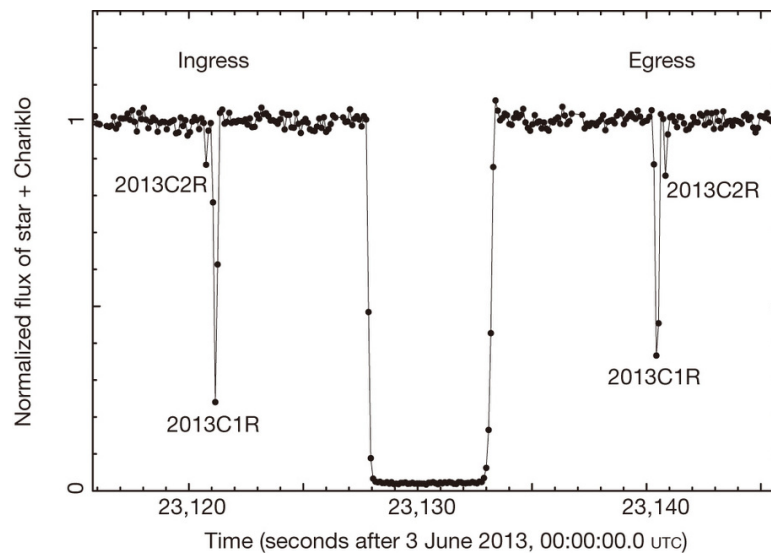
Figure 2.1: Plot of a normalized light curve of the occultation by Chariklo's system. Aperture photometry measured the flux from the target star and a fainter nearby reference star. The central dip is from Chariklo while the two smaller dips on either side are from the rings, C1R and C2R. Source: *Braga-Ribas et al.* [2014].

of 6.16 ± 0.11 km and $3.6 + 1.3, -2.0$ km and optical depths of 0.449 ± 0.009 and $0.05 + 0.06, -0.01$ km, respectively. At egress (after the occultation), the rings have respective widths of 7.17 ± 0.14 km and $3.4 + 1.1, -1.4$ km and optical depths of 0.317 ± 0.008 and $0.07 + 0.05, -0.03$. As shown in the difference in the dip heights in Fig. 2.1, the optical depth for C1R changes by 21% between ingress and egress. This difference is similar to the variations observed in Uranus' narrow rings, so it might be associated with normal mode oscillations that azimuthally modulate the width and optical depth of the rings. The large optical depth of C1R indicates that it is made of significantly more material than C2R [*Braga-Ribas et al.*, 2014], either that C1R is composed of large particles or that it is has small particles that are densely packed.
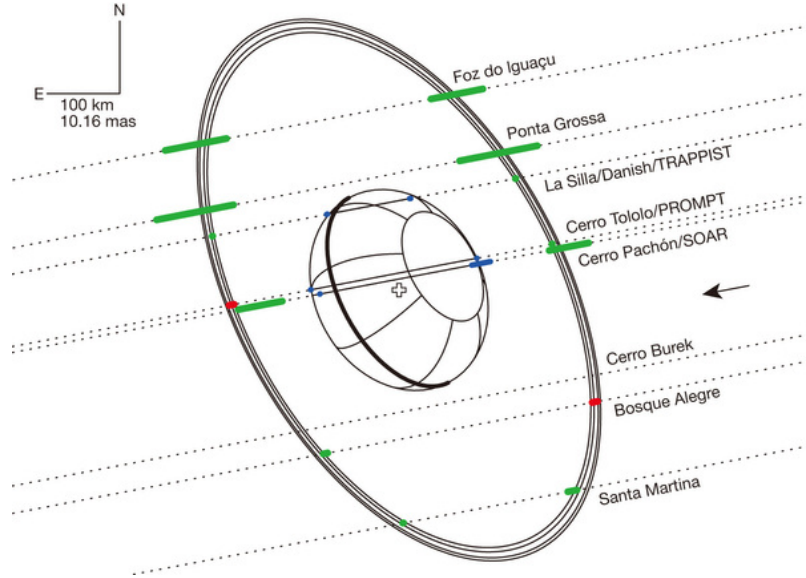

Figure 2.2: Diagram of the orientation of Chariklo's rings. The dotted lines are the star's trajectories relative to Chariklo in the plane of the sky, with the arrow indicating the star's direction of motion. The green segments represent the locations of ring C1R observed at each station. Chariklo's shape is outlined by the blue segments. Source: *Braga-Ribas et al.* [2014].

The orientation of the rings is shown in Fig. 2.2. These rings have an opening angle to the sun of $B = 33.77° \pm 0.41°$, where the opening angle to the sun is defined as the elevation of the sun above the ring plane [*Braga-Ribas et al.*, 2014]. The trajectories of the star relative to Chariklo were collected at several locations along the ring system and a model of the ring system was created by assembling the measurements at each location.

2.3   Characteristics of the Ring Particles

While Chariklo was being observed between 1997 and 2008, the 2 μm water-ice absorption band at its surface disappeared, which indicated that the rings were partly composed of water-ice [*Braga-Ribas et al.*, 2014]. Photometric and spectroscopic measurements were taken of Chariklo and its ring system. From these measurements, models of light scattering to fit the visible and near-infrared spectra were created to obtain information on the composition of both the surface of Chariklo and its rings. The models show that the rings are composed of 20% water ice, $40 - 70\%$ silicates, and $10 - 30\%$ tholins. The particle sizes are roughly 100 μm in radius [*Duffard et al.*, 2014].

2.4   Perturbing Forces

The long-term evolution of small particles' orbits is affected most by non-gravitational forces such as radiation forces and collisions. Small dust grains repel from the Sun by radiation pressure due to momentum carried in solar photons. The orbits of these particles are also affected by the velocity-dependent Poynting-Robertson effect (PR drag). Both solar radiation pressure and PR drag are modeled in Eq. 2.1 for a particle of mass m and geometrical cross section A moving with velocity $\mathbf{v}$ through a radiation field of energy flux density S [*Burns et al.*, 1979].

$$m\dot{\mathbf{v}} = (SA/c)Q_{pr}(a)[(1 - \dot{r}/c)\hat{\mathbf{S}} - \mathbf{v}/c] \tag{2.1}$$

$\hat{\mathbf{S}}$ is a unit vector in the direction of the incident radiation, $\dot{r}$ is the particle's radial velocity, a is the particle radius, and c is the speed of light. Q_{pr} is the size-dependent efficiency factor for radiation pressure and can be calculated from Mie Theory assuming that the particles are homogeneous spheres [*Gustafson*, 1994].

Poynting-Robertson drag is the second term in Eq. 2.1. It causes the dust particles to lose energy and angular momentum [*Burns et al.*, 1979]. This force causes meter-size particles and smaller to migrate towards the Sun as their energy and angular momentum dissipate on time-scales of a few million years [*Braga-Ribas et al.*, 2014; *Goldreich and Tremaine*, 1979].

2.4.1 Solar Radiation Pressure

Solar radiation pressure perturbs a dust particle's orbit [*Gustafson*, 1994]. When a perfectly absorbing particle is located at a point where the energy flux of radiation is S, it intercepts an energy per unit time equal to $\Delta \Sigma = SA$. At the same time, due to transfer of linear momentum the particle experiences a net force directed outward along the radiation source-particle. This force is given as

$$\mathbf{F}_r = \frac{SA}{c}\hat{\mathbf{S}}. \tag{2.2}$$

The absorbed energy heats the grain, but a particle is never a perfect absorber since diffraction implies the particle may interact with an electromagnetic wave in a region much larger than its geometrical cross section [*Mignard*, 1984]. Therefore, Eq. 2.2 is rewritten as

$$\mathbf{F}_r = \frac{SAQ_{pr}(a)}{c}\hat{\mathbf{S}}, \tag{2.3}$$

which is the same as the first term in Eq. 2.1, also known as the radial term where Q_{pr} is the light-scattering efficiency [*Burns et al.*, 1979; *Gustafson*, 1994].

Because both the gravitational force of the Sun and radiation pressure force are proportional to $1/r^2$, the radiation pressure force is often represented as a dimensionless quantity (see Eq.2.4) comparing the two forces so as to eliminate the dependency on the distance from the Sun [*Burns et al.*, 1979; *Gombosi et al.*, 2015; *Mignard*, 1984]. The expression for radiation pressure is

$$\beta_a = \frac{F_r}{F_g} \approx \frac{6 \times 10^{-5} Q_{pr}(a)}{a\rho_a} \tag{2.4}$$

where ρ_a is the characteristic bulk density of the dust particles. In addition to the radius of the grain, β_a is a function of the material composition as well as the surface properties of the grains [*Burns et al.*, 1979]. Particles with radii $a > a_0$ nm have a Q_{pr} that approaches a constant ($Q_{pr} \approx 0.25$), so β_a depends only on $1/a$. β_a can be redefined as β, which is

$$\beta = \begin{cases} \beta_0 y e^{(1-y)} & y \leq 2 \\ 4(\beta_0/e)/y & y > 2 \end{cases} \tag{2.5}$$

where β_0 is the maximum value at a specified radius a_0 and $y = a/a_0$ [*Gombosi et al.*, 2015]. Figure 2.3 shows β for $\beta_0 = 1$ and $a_0 = 100$ nm, which captures the characteristic behavior of ice/silica particles. Since the rings are comprised of mainly silicates and water-ice, this β distribution is sufficient. For particles composed of material other than ice/silica, β would peak at a different particle radius [*Burns et al.*, 1979; *Gombosi et al.*, 2015].
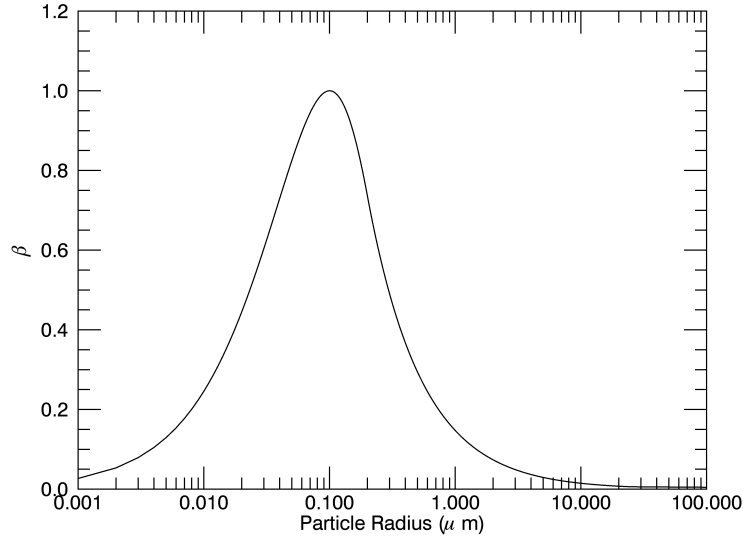

Figure 2.3: Plot of β as a function of particle radius, a. The maximum normalized value of β, or β_0, is set at a = 0.1 μm.

2.5   Background on Shepherd Moons

Rings can be confined by gravitational torques from a series of small satellites, known as shepherd moons, that orbit within the ring system. A satellite can resist tidal disruption at the location of the rings if it is fairly dense, $\rho \geq 2$ g cm^{-3}, or small, $R_s \leq 100$ km [*Goldreich and Tremaine*, 1979].

Let's assume that we have a system in which a ring and satellite orbit are circular. If the satellite is separated from the ring by a distance x, then it exerts a gravitational torque T_s that

repels the ring:

$$T_s \sim \pm f_1 \frac{G^2 m_s^2 r \sigma \Delta r}{\Omega^2 x^4} \tag{2.6}$$

where m_s is the mass of the shepherd moon, σ is the density of the ring and is assumed to be uniform, Δr is the ring width, Ω is the orbital angular velocity, and f_1 is of order unity. The + and - signs indicate that the satellite is either inside or outside the ring, respectively [*Goldreich and Tremaine*, 1979].

Particles between two satellites will be formed into a ring on which the external force is zero. The external torque deposits angular momentum in the inner part of the ring and removes it from the outer part. In other words, a satellite on the inside of the ring has a gravitational influence that speeds up particles and pushes them into higher orbit and back into the main body of the ring. The opposite occurs for a satellite located outside of the ring, in which its gravitational influence slows particles down and pushes them into lower orbit [*Goldreich and Tremaine*, 1979].

2.5.1   Dynamics of a Shepherded Dust Ring

Encounters between ring particles and satellites are relatively quick, lasting on the order of one rotation period, while the interval between such encounters is ~ 100 times longer [*Showalter and Burns*, 1982]. As a result, particles mostly experience perturbations due to solar radiation pressure with an occasional gravitational "kick" from the satellites to modify their orbital elements.

The simplest case is of a shepherd moon in a circular orbit near a narrow circular ring. As shown in Fig. 2.4, as each ring particle passes by the satellite, it gets scattered gravitationally onto a new, slightly eccentric orbit. It is thereafter observed to follow a sinusoidal path in the rotating frame fixed with the satellite [*Showalter and Burns*, 1982].
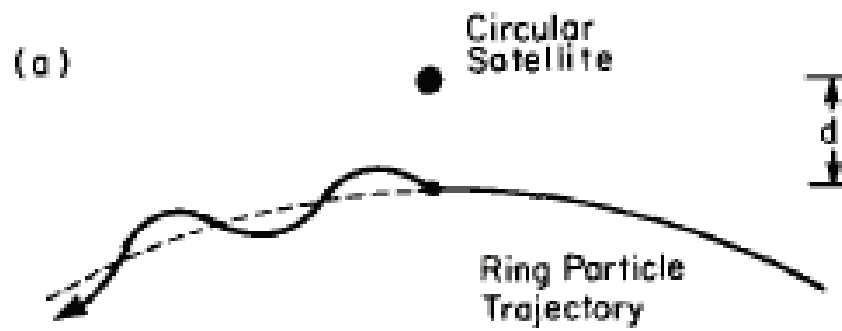
Figure 2.4: This image shows the perturbation of a ring particle trajectory by a nearby satellite. The distance between the satellite and the ring system is d. The reference frame is fixed with respect to the satellite [*Showalter and Burns*, 1982].

Chapter 3

Dynamics in 2D

These next two chapters introduce two models to simulate Chariklo's ring system. For both models, we simulated a particle beginning at a radial distance of 3.15 Chariklo radii, which is where Chariklo's inner ring is located. The particle was composed of ice/silica with a radius of 100 µm, which describes the types of particles comprising the rings. The only perturbing force considered in both of the models was solar radiation pressure. Because PR drag does not have a significant impact on the lifetime of a particle 100 µm or smaller in radius until after a few million years, we did not consider it. We also did not consider solar wind drag because it affects the particles in the same direction as solar radiation pressure. Interparticle collisions were too difficult to numerically simulate and were not significant enough to include them in the problem.

3.1   Model Set-up

In the case of the 2-D model shown in Fig. 3.1, Chariklo remains stationary at the origin of an x-y plane while a single dust particle of size $a = 100\,\mu$m orbits it in this plane. The forces impacting the particle's orbit are Chariklo's gravity and solar radiation pressure. The gravitational force from the Sun is neglected.

The equations of motion for this system (see Eq. 3.1) can be broken into x- and y- components with radiation pressure constantly being applied in the + x-direction.

$$\ddot{\mathbf{x}}(\mathbf{x}, t) = -\frac{Gm}{r^2}\hat{\mathbf{x}} + \beta\frac{GM}{d^2}\hat{\mathbf{x}} \tag{3.1a}$$

$$\ddot{\mathbf{y}}(\mathbf{y}, t) = -\frac{Gm}{r^2}\hat{\mathbf{y}} \tag{3.1b}$$

We define M as the mass of the Sun, m as Chariklo's mass, r as the radial distance between the dust particle and Chariklo, and d as the distance between the Sun and the dust particle. With reference to Fig. 3.1, $r = |\mathbf{r_2}| = \sqrt{x^2 + y^2}$ and $d = |\mathbf{r_1}|$.

At $t = 0$, the particle is located on the x-axis, which in polar coordinates translates to $\mathbf{r}(0) = r\cos\phi = r$ setting $\phi = 0$. The initial velocity of the particle is in the y-direction, represented as $\dot{\mathbf{r}}(r, 0) = \dot{r}\sin\phi + r\dot{\phi}\cos\phi = r\dot{\phi}$.
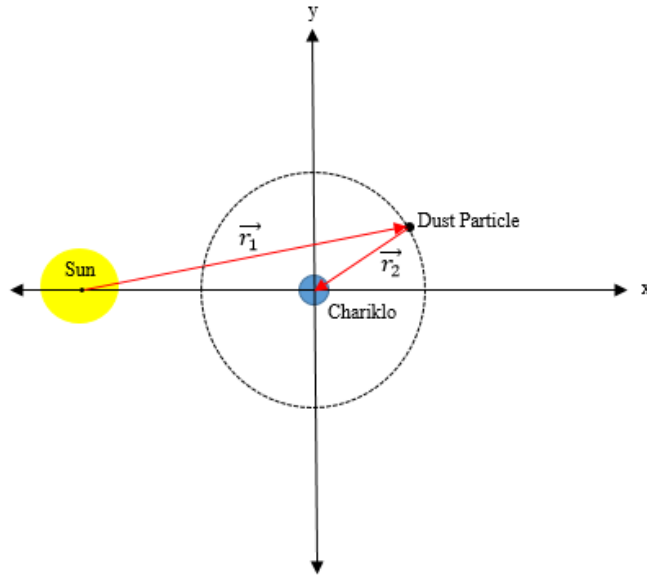

Figure 3.1: 2D model of the Chariklo system including the Sun. The vectors $\mathbf{r_1}$ and $\mathbf{r_2}$ indicate the displacement between the Sun and the dust particle and Chariklo and the dust particle, respectively. The dashed ring around Chariklo is a model of the dust particle's orbit. Image is not to scale.

A particle's orbit, shown in Fig. 3.2, was numerically integrated using Eq. 3.1. A Fortran-based numerical step integrator called LSODE was used, and the lifetime of the particle was monitored by stopping the integration when the particle collided into Chariklo. We tracked the particle's pericenter verifying that the numerical integration stopped when the particle collided into Chariklo, as shown in Fig. 3.6.

3.2 Simulated Results against Theory

3.2.1 Keplerian Orbital Elements

Our results are easily described using Keplerian elements:

$$a = -\frac{Gm}{2E} \tag{3.2}$$

$$e = \sqrt{1 + \frac{2(\mathbf{J}')^2 E}{Gm}} \tag{3.3}$$

where a is the semi-major axis and e is the eccentricity. E is the particle's specific orbital energy defined by $E = v^2/2 - Gm/r$. There is a negative sign in Eq. 3.2 because the specific orbital energy is negative. $\mathbf{J}'$ is the particle's specific angular momentum [*Burns*, 1976], so $\mathbf{J}' = \mathbf{r} \times \mathbf{v}$.

As a particle travels in the -x-direction, or in the opposite direction to solar radiation pressure force, it loses energy, but it gains energy back as it travels in the same direction as the force. Hence, a particle's orbital energy is conserved as it experiences solar radiation pressure because the work done on its orbit by the force is zero. The black curve in Fig. 3.3 verifies that orbital energy is conserved. The small deviation from $E/E_0 = 1$ is due to numerical error accumulation.

A particle in orbit about a central object experiences a change in torque due to solar radiation pressure. Torque is defined by $\boldsymbol{\tau} = \mathbf{r} \times \mathbf{f}$ where $\mathbf{r}$ is the radial position vector of the particle and $\mathbf{f}$ is the specific solar radiation pressure force. A particle traveling around Chariklo begins in a circular orbit and quickly becomes elongated along the y-direction, as shown in Fig. 3.2. The radial position vector along the y-axis is perpendicular to the radiation pressure force that is constantly being applied in the x-direction. Since torque is active over time and is related to angular momentum by $\mathbf{J}' = \int \boldsymbol{\tau} dt$, the orbit's angular momentum isn't conserved. The green curve in Fig. 3.3 shows that angular momentum is lost over the orbital lifetime of a particle.

The perturbation equations for the Kepler elements averaged over an orbital period help determine the lifetime of a particle's orbit. Only three elements are needed to describe the orbital path and shape of the trajectory. When $e << 1$, they are:

$$\left\langle \frac{da}{dt} \right\rangle = 0 \tag{3.4a}$$
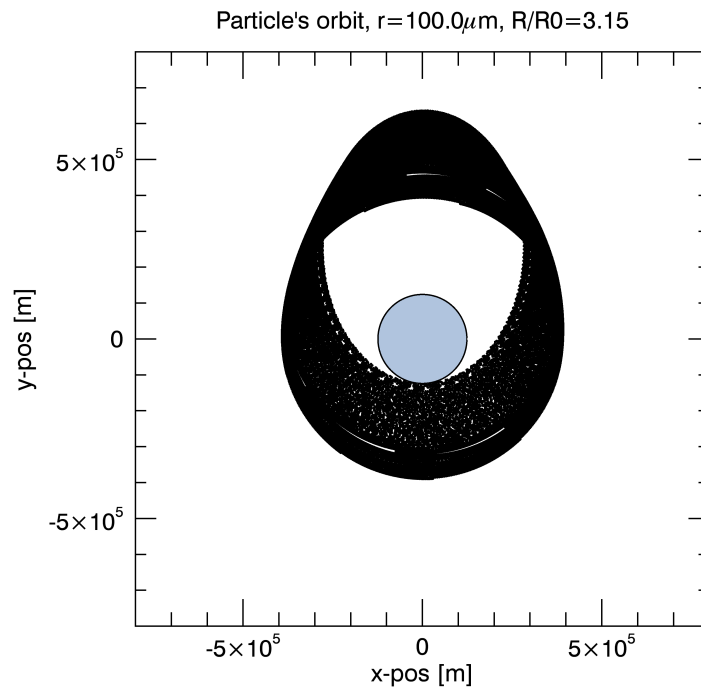
Figure 3.2: A single dust particle's perturbed orbit before it crashes into Chariklo. Chariklo is the blue circle at the origin. The Sun is located on the x-axis 15.8 AU to the left of Chariklo's system.
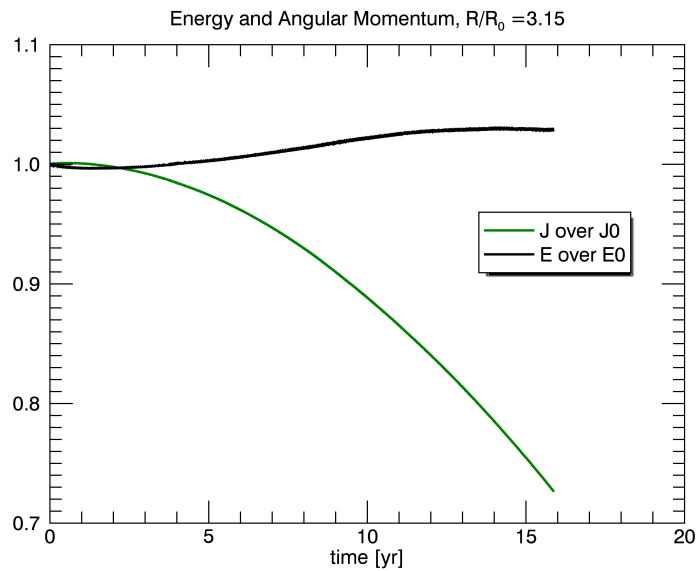

Figure 3.3: Plot of the final over initial angular momentum and final over initial orbital energy for a particle's orbit.

$$\left\langle \frac{de}{dt} \right\rangle = \lambda \sin \tilde{\omega} \tag{3.4b}$$

$$\left\langle \frac{d\tilde{\omega}}{dt} \right\rangle = \frac{\lambda}{e} \cos \tilde{\omega} \tag{3.4c}$$

where $\tilde{\omega}$ is the longitude of pericenter or the angle measured from the Sun's direction counter-clockwise (as viewed from the North celestial pole) to pericenter [*Horányi and Mendis*, 1991; *Horányi et al.*, 1992].

A particle's orbital energy determines the orbit's semi-major axis a, so Eq. 3.4a equals zero because the orbital energy does not change over time. Hence, the semi-major axis is constant over time, as shown in Fig. 3.4. For a particle starting in a circular orbit, $e \approx 0$. Plugging that into Eq. 3.4c results in an undefined longitude of pericenter's time rate of change. The only way Eq. 3.4c isn't undefined is if we set it to zero, meaning that $\tilde{\omega} = \pm\frac{\pi}{2}$. Hence, Eq. 3.4 simplifies to:

$$\left\langle \frac{da}{dt} \right\rangle = 0 \tag{3.5a}$$

$$\left\langle \frac{de}{dt} \right\rangle = \lambda \tag{3.5b}$$

$$\left\langle \frac{d\tilde{\omega}}{dt} \right\rangle = 0 \tag{3.5c}$$

where $\lambda = \frac{3hf}{2Gm}$, and $h = \sqrt{Gma}$ and $f = \beta\frac{GM}{d^2}$. For a given particle size with a given distance from the Sun, $\lambda = \gamma\sqrt{a}$ where $\gamma = \frac{3M\sqrt{Gm}\beta}{2md^2}$. In this case, λ is constant, which explains the eccentricity in Fig. 3.5 growing linearly with time. As shown in Fig 3.6, the orbital pericenter decreases linearly in time because it is related to eccentricity by $r_p = a(1-e)$, while the apocenter increases because it is equal to $r_a = a(1+e)$.

The particle collides into Chariklo at maximum eccentricity, so $a(1-e_{max}) = R_0$ where R_0 is the radius of Chariklo. Solving for e_{max}, we find $e_{max} = 1 - \frac{R_0}{a}$, which is the analytical solution plotted in Fig. 3.5. The lifetime of a particle's orbit is defined by $t_{life} = e_{max}/\left\langle \frac{de}{dt} \right\rangle$. The lifetime of the particle's orbit is rewritten as

$$t_{life} = \frac{1 - \frac{R_0}{a}}{\gamma\sqrt{a}}. \tag{3.6}$$

Eq. 3.6 helps to solve for the lifetime of a particle at varying radial distances from Chariklo. If we know γ, we can use Fig. 3.7 to determine the lifetime of a particle at a specific semi-major
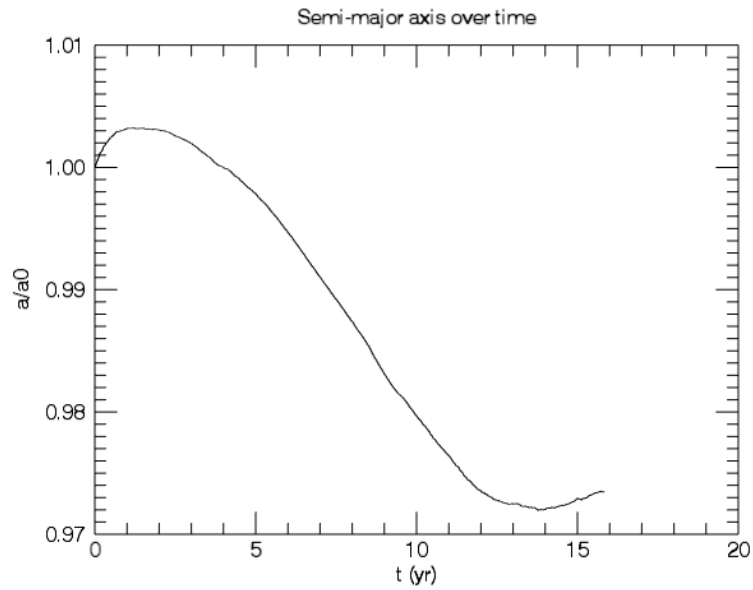
Figure 3.4: The semi-major axis was monitored as a 100 µm dust particle orbited Chariklo beginning at $R/R_0 = 3.15$. It is expected that the semi-major axis remains constant over time, so the small deviation is due to numerical error accumulation.
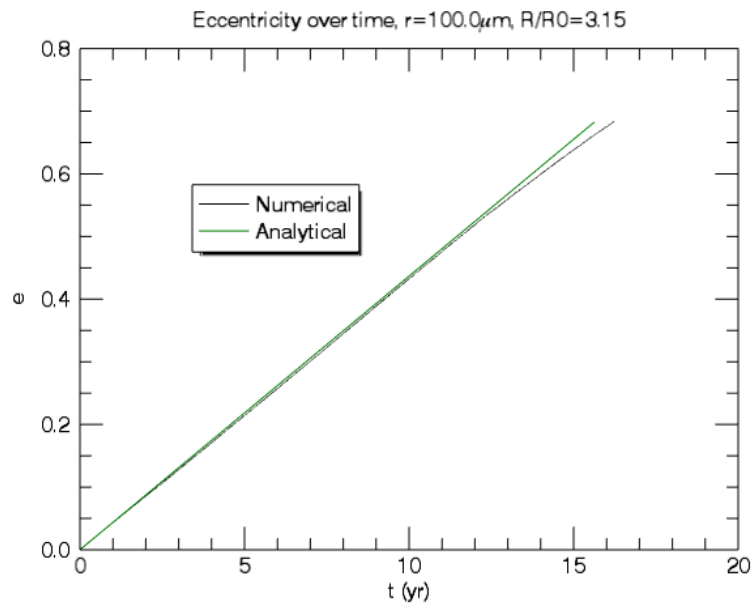

Figure 3.5: Plot of the eccentricity of the dust particle's orbit. It indicates a highly elliptic orbit at the end of the particle's orbital lifetime.
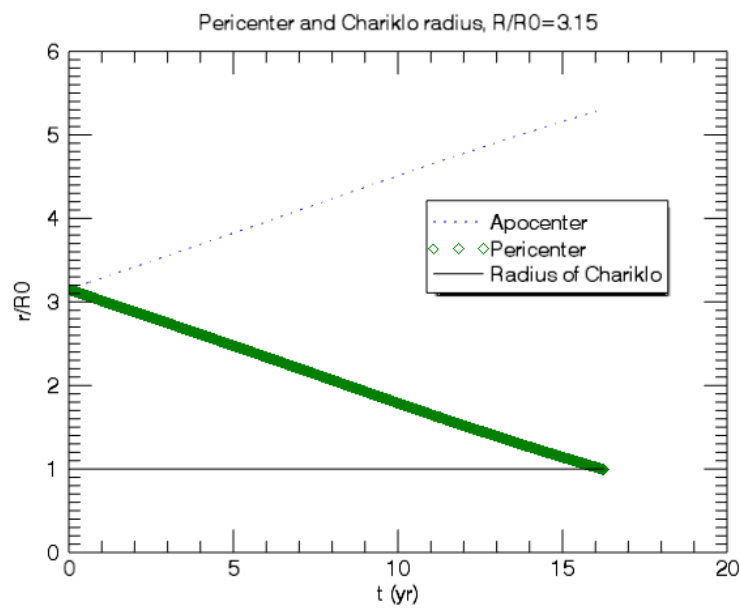
Figure 3.6: Plot of the apocenter and pericenter over the lifetime of a particle's orbit. The horizontal line corresponds to Chariklo's radius R_0. The y-axis is a ratio of r/R_0, where r is the particle's radial distance from Chariklo.

axis. For a $100\,\mu\text{m}$ particle, $\gamma \approx 2.155 \times 10^{-12}$. The lifetime of a particle as a function of its initial radial distance can then be plotted using the known value for γ. Fig. 3.8 shows both the analytical and numerical solutions of lifetime peaking where the rings are observed ($\sim 3R_0$).
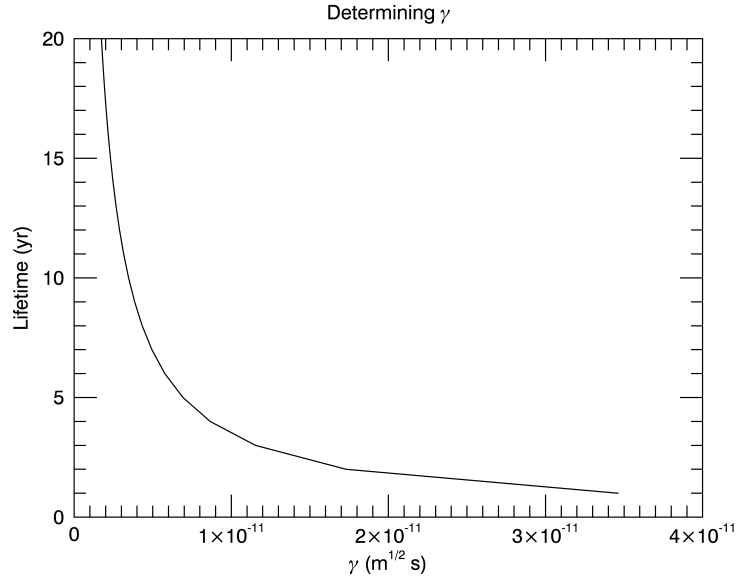

Figure 3.7: Plot of gamma as a function of orbital lifetime. The semi-major axis was set at $a = 3.15R_0$.

Fig. 3.9 verifies that the computational simulations agree with the analytical theory. Analytically, the lifetime for the varying particle radii in Fig. 3.9 was found by evaluating Eq. 3.6 for several β values. The numerical values were taken by integrating a single dust particle for several particle radii. This figure shows that ice/silica particles $100\,\mu\text{m}$ in radius remain in orbit the longest.

3.3   Simulating a Ring System

The orbital dynamics of a single particle is characteristic of a ring system, but it is useful to model a ring system comprised of several particles when considering the impacts of external forces, such as shepherd moons. To simulate a ring system composed of 100 particles, the model in this chapter is modified by numerically integrating 100 particles' orbits, with the first particle
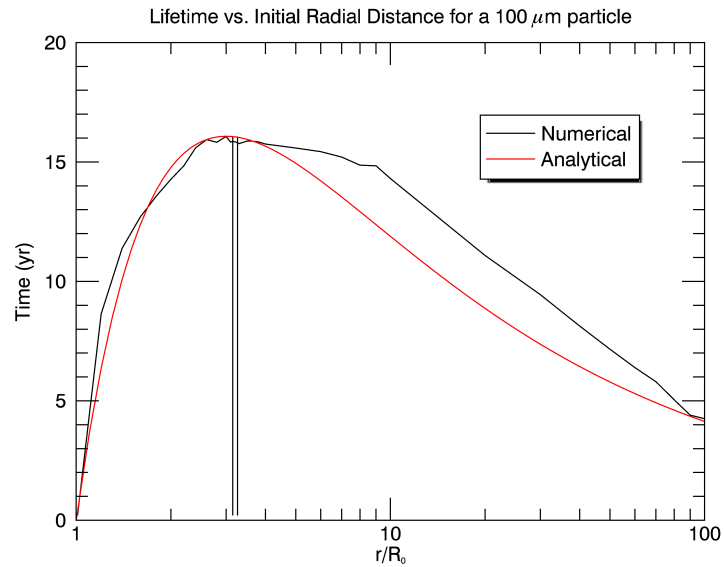
Figure 3.8: Plot of lifetime of a $100\,\mu$m dust particle of varying initial radial distance. The two vertical lines represent the radial distance at which the rings are observed.
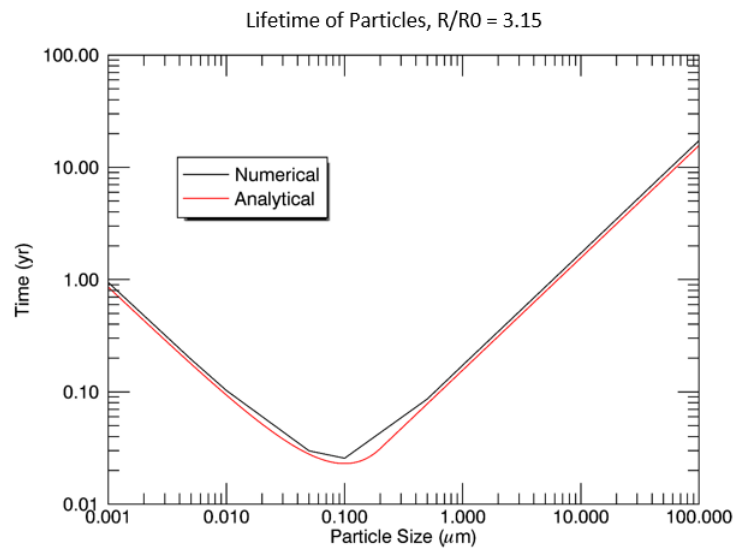

Figure 3.9: Plot of the lifetime of a dust particle of varying radius at a fixed initial radial distance. As shown in this figure and in Figure 2.3, the largest β corresponds to the shortest lifetime.

positioned at $3R_0$ and each subsequent particle located $+3$ km away from the last. The numerical integration updates a particle's position by one step, and then goes to the next particle to move it one step. The process continues until all of the particles have moved a single step, and then the loop goes back to the first particle to move it a second step. This continues until all of the particles collide into Chariklo. Updating the particles' position in this way made it simple to take snapshots of the ring system at various points in time. The first image in Fig. 3.10 shows the initial spreading of the particles as they began their orbits, and the last image shows most of the particles gathered at the bottom of Chariklo where they had collided into the minor planet. Further work can be done on this model by including particles of different sizes and compositions to determine how the orbital dynamics change for different types of particles.
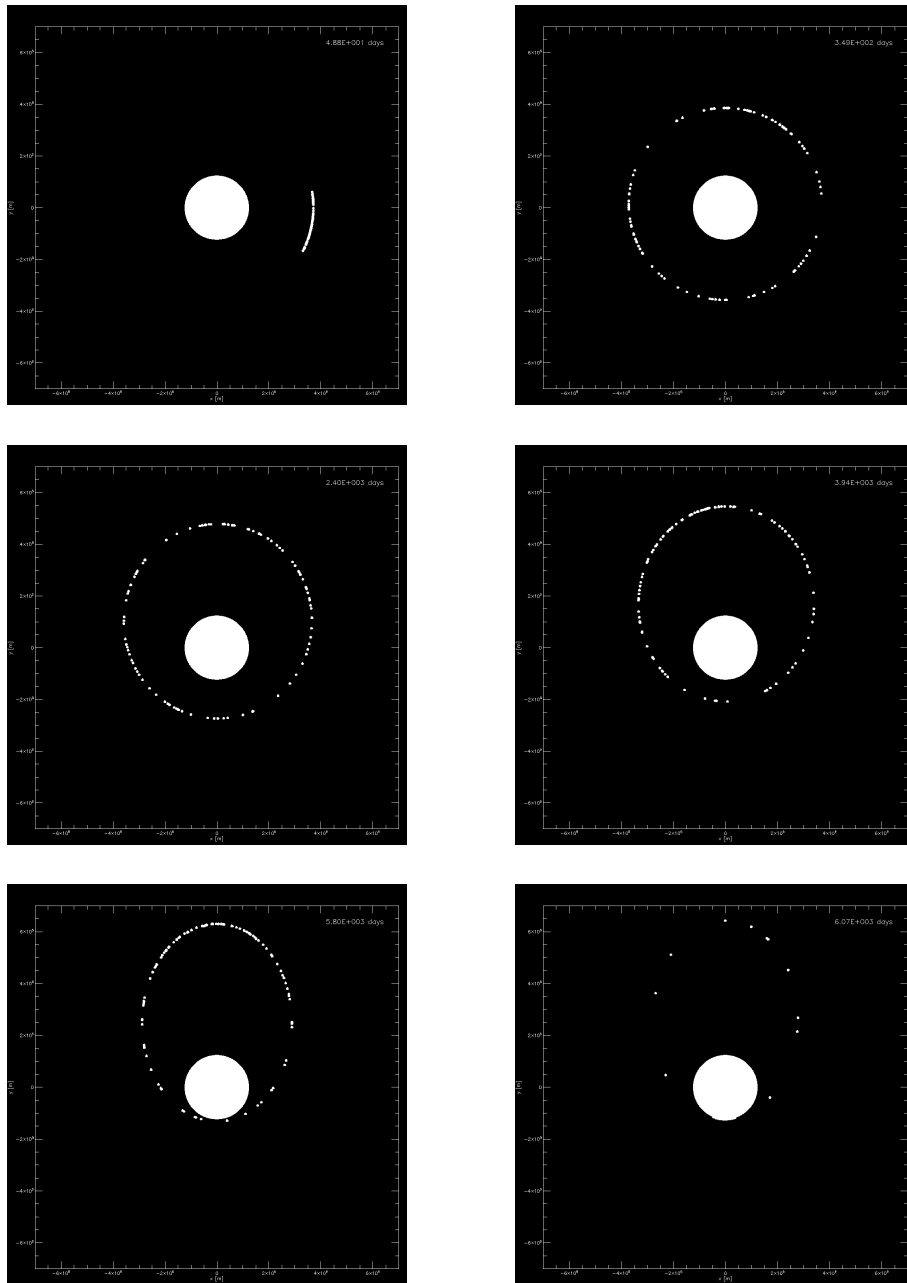
Figure 3.10: Snapshots of the ring system comprised of 100 particles as it evolves over time. The white filled circle is Chariklo.

Chapter 4

Dynamics in 3D

4.1   Model Set-up

In this model (See Fig. 4.1), Chariklo is at the origin with the ring plane in the xy-plane.
The Sun is located at an opening angle $B = 33.17°$ in the xz-plane. Like in the 2D model, the forces
impacting a dust particle's orbit are Chariklo's gravitational force and solar radiation pressure.
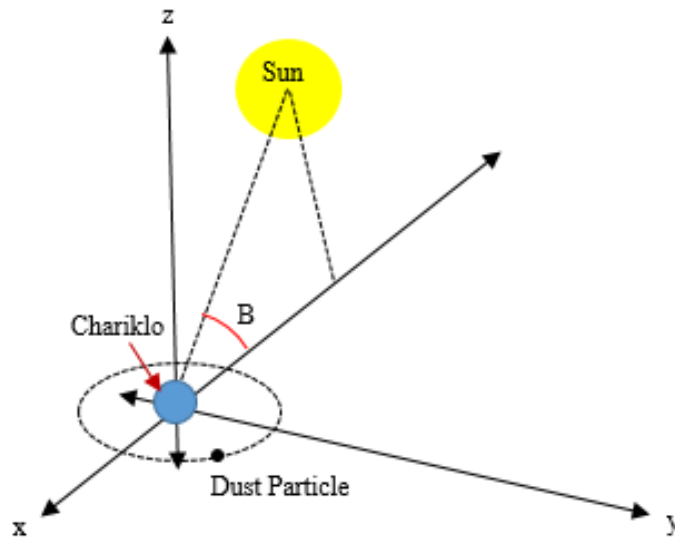

Figure 4.1: 3D model of the Chariklo system including the Sun. The ring plane is in the xy-plane
so that the opening angle B of the Sun is the elevation above the xy-plane. The dashed ring around
Chariklo is a model of the dust particle's orbit. Image is not to scale.

The equations of motion for this system can be written in x-, y-, and z- components with the

radiation pressure force acting on the particle in both the x and z directions:

$$\ddot{\mathbf{x}}(\mathbf{x}, t) = -\frac{Gm}{r^2}\hat{\mathbf{x}} + \beta\frac{GM\cos{(B)}}{d^2}\hat{\mathbf{x}} \tag{4.1a}$$

$$\ddot{\mathbf{y}}(\mathbf{y}, t) = -\frac{Gm}{r^2}\hat{\mathbf{y}} \tag{4.1b}$$

$$\ddot{\mathbf{z}}(\mathbf{z}, t) = -\frac{Gm}{r^2}\hat{\mathbf{z}} + \beta\frac{GM\sin{(B)}}{d^2}\hat{\mathbf{z}}. \tag{4.1c}$$

In this model, $r = \sqrt{x^2 + y^2 + z^2}$. At $t = 0$, the particle is located on the x-axis with initial velocity in the y-direction. As the particle begins its orbit, the z-component of the radiation pressure causes the particle's orbit to become slightly inclined in the z-direction.

4.2   Results

As the work along the particle's orbit in three dimensions is zero, orbital energy is conserved as shown by the black curve in Fig. 4.2 and the semi-major axis curve in Fig. 4.3. Angular momentum is not conserved for the same reason it is not conserved in two dimensions. When compared to the orbital angular momentum of the particle in 2D, the particle experiencing radiation pressure in both the x- and z- directions loses the same amount of angular momentum over a longer period of time, as shown in Fig. 4.2. Part of the radiation pressure force is acting in the ring plane, while another part is acting perpendicular to the ring plane. Only the force in the ring plane contributes to the torque, meaning that less angular momentum is lost over a given amount of time. The smaller rate of change of angular momentum in this model is apparent in Fig. 4.4, which shows the orbit taking longer to reach maximum eccentricity than in Fig. 3.5.

Because a component of solar radiation pressure acts in the z-direction, the rings become slightly inclined. The Keplerian element i describes the degree of inclination of a particle's orbit in radians and is defined in the following equation

$$i = \cos^{-1}\left(\frac{\mathbf{J}'_{\mathbf{z}}}{\mathbf{J}'}\right) \tag{4.2}$$

where $\mathbf{J}'_{\mathbf{z}}$ is the z-component of the specific angular momentum $\mathbf{J}'$ [*Burns*, 1976]. The inclination component affects the orbital eccentricity so that it no longer linearly increases with time. Despite looking nearly linear, Fig. 4.4 is not a linear plot.

Change in Total Energy, R/R0 =3.15

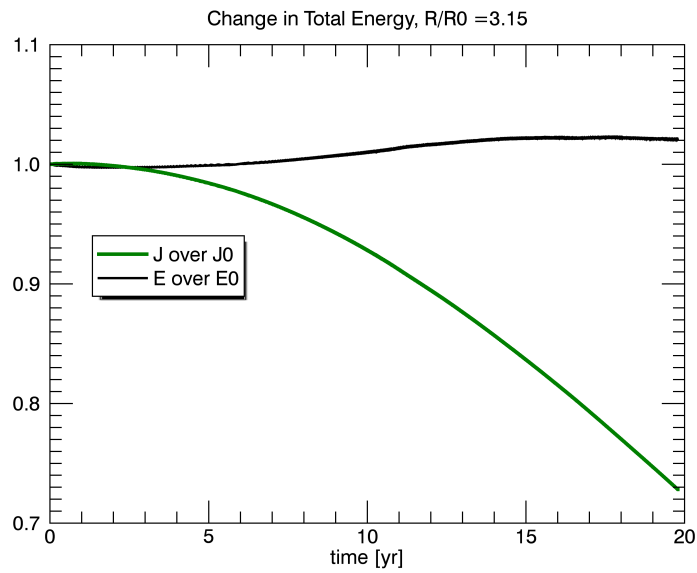Figure 4.2: Plot of the final over initial angular momentum and final over initial orbital energy for a particle's 3D orbit.

Semi-major axis over time

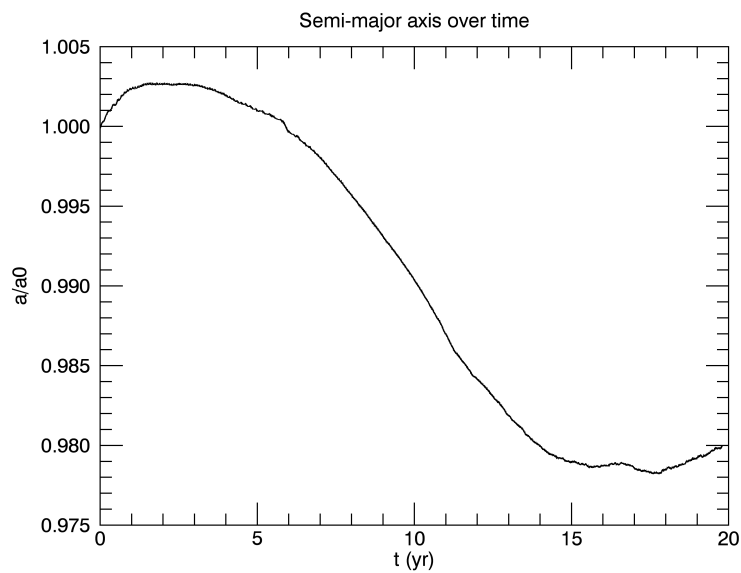
Figure 4.3: The semi-major axis was monitored as a $100\,\mu m$ dust particle orbited Chariklo in 3D beginning at $R/R_0 = 3.15$. It is expected that the semi-major axis remains constant over time, so the small deviation is due to numerical error accumulation.
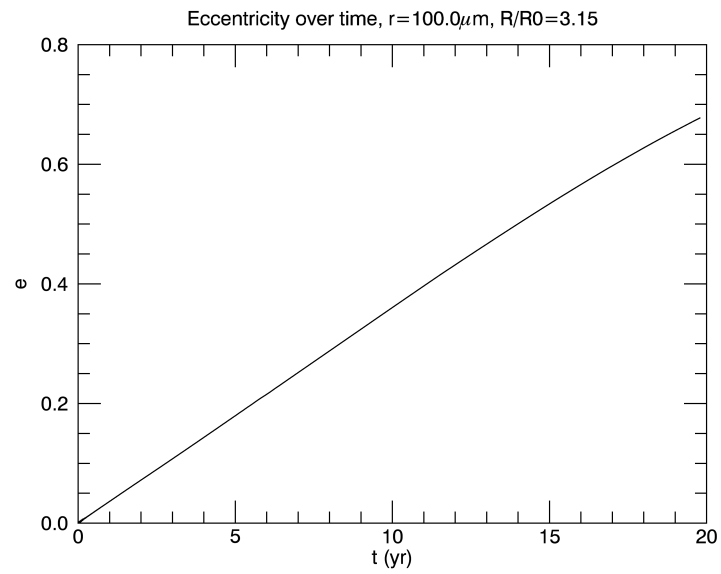
Figure 4.4: Plot of the eccentricity of the dust particle's orbit in 3D.
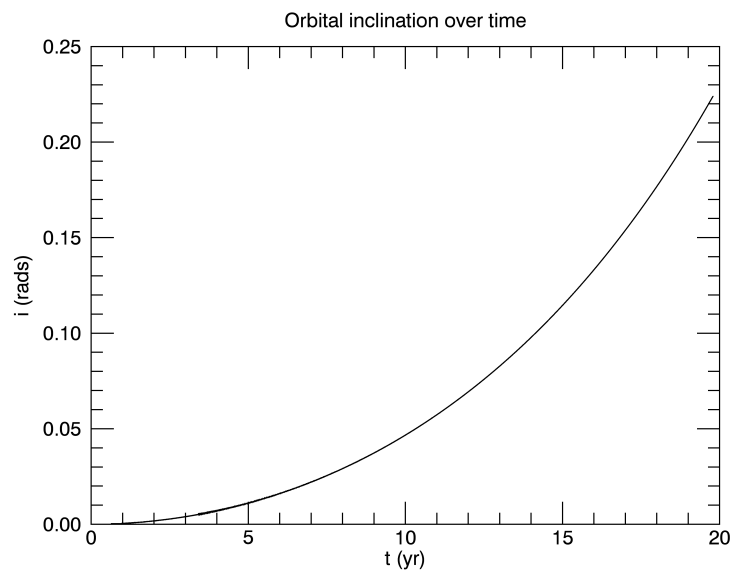
Figure 4.5: Plot of a dust particle's orbital inclination.

There exist no analytic solutions that take into account the inclination of an orbit when determining the orbit's lifetime. We see in Figs. 4.4 and 4.6 that this lifetime is about three years longer than the lifetime in the 2D case. The simulated result is $t_{life} = 19.78$ years.

Figure 4.6: Plot of the apocenter and pericenter for a particle in the 3D model.

Chapter 5

Discussion

5.1   Conclusion

Water-ice and silica particles in orbit about a Chariklo-sized object exhibit the longest lifetime when they are 100 μm in radius and they have a semi-major axis equal to about three Chariklo radii. This supports current observations of the rings' featu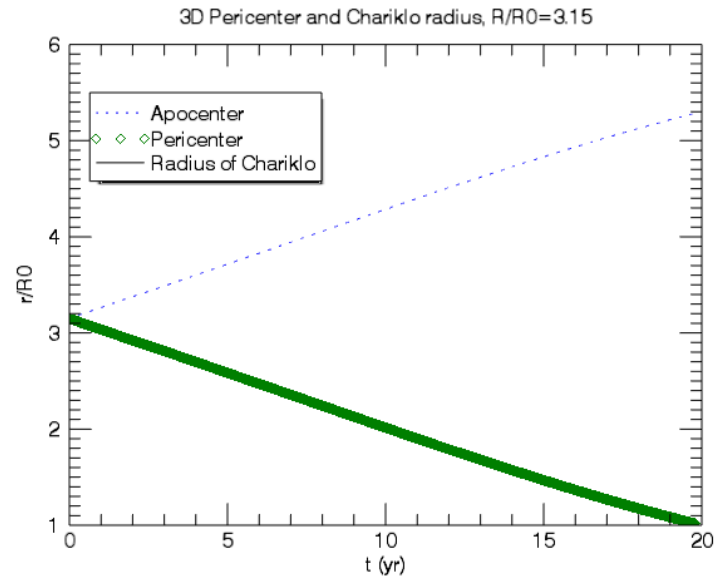res [*Braga-Ribas et al.*, 2014; *Duffard et al.*, 2014]. Yet, the rings' lifetimes are still unknown. While some models suggest that Chariklo's rings formed while Chariklo was still trans-Neptunian less than 10 Mya [*Braga-Ribas et al.*, 2014], current results show that the lifetime of small (100 μm or less in radius) particles in orbit is approximately 20 years due to solar radiation pressure forces. There are a few possible explanations for the apparent contradiction in the lifetime of the rings' orbits.

One possibility is that the ring system's lifetime is on the order of 20 years, so the rings are actually young. After a few thousand years, particles will spread due to interparticle collisions [*Braga-Ribas et al.*, 2014]. This disagrees with the idea that the rings were formed while Chariklo was in the Kuiper belt unless Chariklo drifted into the Solar System less than a few thousand years ago. Unfortunately as Chariklo was not discovered until 1997, our knowledge of how its system has evolved is currently limited.

Another possibility is that the lifetime of a single particle is 20 years, but the ring system is much older than that. Particles can disperse from their orbits but there must then be continual additions into the ring system. This describes an inherently unstable ring system that is continually being replenished by additional sources.

On the other hand, the rings might be actively contained by external forces such as shepherd moons. Two or three shepherd moons would be located in the ring system: one on the inside of the inner ring, one in the gap between the two rings, and/or one outside of the outer ring. Once a particle deviates from its orbit, it can either gain or lose angular momentum from the satellites' gravitational influence. This change in angular momentum pushes it back into orbit around the central object. The satellites themselves lose angular momentum, but their loss is at a much slower rate than the particles' losses from solar radiation pressure.

The dynamics of the simulated ring particles are analogous to perturbed ring particle orbits around planetary objects. Despite not being able to characterize the lifetime of the ring system, these simple models coupled with previous observations show that a dust ring system in orbit around Chariklo is likely. The results from these models can be used to characterize other non-planetary ringed systems.

5.2   Ongoing Research

While we have photometric and spectroscopic evidence of the compositions and sizes of the ring particles [*Duffard et al.*, 2014], these observations could be tested by characterizing the particles with an optical depth profile (See Appendix A). An optical depth profile can be created from this probability by the following equation:

$$\tau(r) = \int \pi a^2 N(r) dx \tag{5.1}$$

where a is the particle radius and N(r) is the number of particles in a dxdydz volume element [*Cuzzi*, 1985]. In order to do this calculation, we wouldn't integrate over the radial distance, which is shown in Appendix A. Instead, we would integrate to generate a 1D density profile similar to an edge-on ring measurement. Chariklo's inner ring has an optical depth of 0.4, which is quite large. It would be useful to create an optical depth profile to determine if the ring is composed of several small particles that are densely packed or if it is composed of larger, more spaced out particles.

In Chapter 3.3, I described a system comprised of 100 equal-sized particles. For future work, I

intend to create a ring analogous to the currently observed rings. This ring would contain multiple-sized particles composed of water-ice, silicates, and tholins. I then plan to implement shepherd moons into the simulation to determine how long a confined ring system could be sustained. The shepherd moons would be on the order of 100 m to 1 km in radius and be a few kilometers away from the rings [*Goldreich and Tremaine*, 1979]. Because there are currently observational limits for finding satellites within Chariklo's ring system, this future work could be the first steps toward determining whether or not Chariklo's ring system contains satellites.

Bibliography

Belskaya, I. N., S. Bagnulo, M. A. Barucci, K. Muinonen, G. P. Tozzi, S. Fornasier, and L. Kolokolova (2010), Polarimetry of Centaurs (2060) Chiron, (5145) Pholus and (10199) Chariklo, *Icarus*, *210*, 472–479, doi:10.1016/j.icarus.2010.06.005.

Braga-Ribas, F., et al. (2014), A ring system detected around the Centaur (10199) Chariklo, *Nature*, *508*, 72–75, doi:10.1038/nature13155.

Burns, J. A. (1976), Elementary derivation of the perturbation equations of celestial mechanics, *American Journal of Physics*, *44*, 944–949.

Burns, J. A., P. L. Lamy, and S. Soter (1979), Radiation forces on small particles in the solar system, *Icarus*, *40*, 1–48, doi:10.1016/0019-1035(79)90050-2.

Cuzzi, J. N. (1985), Rings of Uranus - Not so thick, not so black, *Icarus*, *63*, 312–316, doi: 10.1016/0019-1035(85)90014-4.

Delsanti, A., and D. Jewitt (2006), *The Solar System Beyond The Planets*, pp. 267–293, Springer-Verlag, Berlin, Heidelberg, doi:10.1007/3-540-37683-6_11.

Duffard, R., et al. (2014), Photometric and spectroscopic evidence for a dense ring system around Centaur Chariklo, *Astron. & Astrophys.*, *568*, A79, doi:10.1051/0004-6361/201424208.

Fornasier, S., D. Lazzaro, A. Alvarez-Candal, C. Snodgrass, G. P. Tozzi, J. M. Carvano, Y. Jiménez-Teja, J. S. Silva, and D. M. Bramich (2014), The Centaur 10199 Chariklo: investigation into rotational period, absolute magnitude, and cometary activity, *Astron. & Astrophys.*, *568*, L11, doi:10.1051/0004-6361/201424439.

Goldreich, P., and S. Tremaine (1979), Towards a theory for the Uranian rings, *Nature*, *277*, 97–99, doi:10.1038/277097a0.

Gombosi, T. I., J. L. Burch, and M. Horányi (2015), Negatively charged nano-grains at 67P/Churyumov-Gerasimenko, *Astron. & Astrophys.*, *583*, A23, doi:10.1051/0004-6361/201526316.

Guilbert-Lepoutre, A. (2011), A Thermal Evolution Model of Centaur 10199 Chariklo, *Astron. J.*, *141*, 103, doi:10.1088/0004-6256/141/3/103.

Gustafson, B. A. S. (1994), Physics of Zodiacal Dust, *Annual Review of Earth and Planetary Sciences*, *22*, 553–595, doi:10.1146/annurev.ea.22.050194.003005.

Horányi, M., and D. A. Mendis (1991), The electrodynamics of charged dust grains in the cometary environment, *Comets in the Post-Halley Era (eds.: R.L. Newburn, M. Neugebauer and J. Rahe)*, *2*, 1093–1104.

Horányi, M., J. Burns, and D. Hamilton (1992), The dynamics of Saturn's E ring particles, *Icarus*, *97*, 248–259, doi:10.1016/0019-1035(92)90131-P.

Horner, J., N. W. Evans, and M. E. Bailey (2004), Simulations of the population of Centaurs - I. The bulk statistics, *MNRAS*, *354*, 798–810, doi:10.1111/j.1365-2966.2004.08240.x.

Hyodo, R., S. Charnoz, H. Genda, and K. Ohtsuki (2016), Formation of Centaurs' rings through their partial tidal disruption during planetary encounters, *The Astrophysical Journal Letters*, *828*, L8, doi:10.3847/2041-8205/828/1/L8.

Mignard, F. (1984), Effects of radiation forces on dust particles in planetary rings, in *IAU Colloq. 75: Planetary Rings*, edited by R. Greenberg and A. Brahic, pp. 333–366.

Showalter, M. R., and J. A. Burns (1982), A numerical study of Saturn's F-ring, *Icarus*, *52*, 526–544, doi:10.1016/0019-1035(82)90013-6.

Appendix A

Radial Distribution Profiles

This is preliminary research for creating an optical depth profile for a single particle orbiting Chariklo.

When radiation propagates through a volume containing ring particles, measuring the amount of matter that is encountered is important for characterizing the ring system. Determining the optical depth of the ring system yields its density as well as the absorption, emission, and scattering properties of the particles. From these optical properties, we can determine the ring's composition.

Spatial density $\rho(r)$ of a single dust particle in orbit about Chariklo is a function of its radial distance from Chariklo. It is defined as $\rho(r) = N/V$, where N is the sum of how many particles are at a given radial distance multiplied by how long they remain at that given distance. V is the volume of the torus (ring), which is the space over which the particles are spread. Fig. A.1 is an azimuthally averaged radial profile, meaning that the density is integrated over radial distance. The y-axis gives the probability that a single particle will be in a certain location along the ring system in a unit of time.

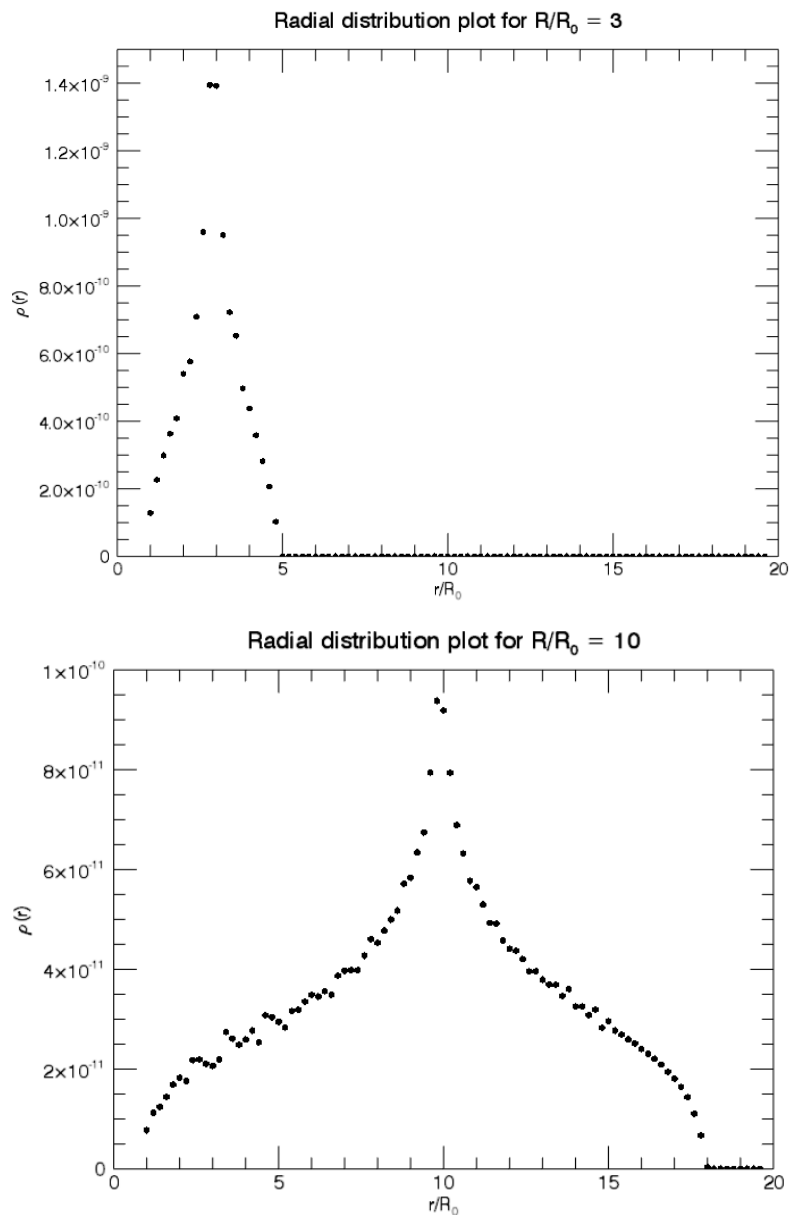Figure A.1: (a) and (b) Radial distribution plots showing the spatial density of one $100\,\mu\text{m}$ dust particle at given radial distances from Chariklo. The densest location is where the particle's orbit begins. The difference in shape between the two graphs is dependent upon the difference in the particles angular momentum at $R = 3$ and at $R = 10$. Description of the y-axis is in the text.

Code For Simulating Dust Dynamics in 3D

The following is a sample of the code that I wrote for the 3D model of a single particle orbiting Chariklo.

```
FUNCTION FORCE3D, X, Y


  ;; Description:
  ;;    Gravitational and radiation pressure forces impact particle orbiting
  ;;    Chariklo
  ;; Integration:
  ;;    Using built−in variable step−size function LSODE
  ;; Frame:
  ;;    Chariklo centered at origin in cartesian coordinates
  ;;    Sun in x−z plane, 33.77 degree−inclination in z−axis
  ;; Author: Juliet Pilewskie


  ; COMMON test, rd


  ;; CONSTANTS
  M_sun = 1.9891e30 ; mass of sun (kg)
```

```
M_centaur = 8.4e18 ; mass of Chariklo (kg)

G = 6.67e-11 ; m^3 kg^(-1) s^(-2)

AU = 1.49598e11 ; m

Rchar = 1.24e5 ; Radius of centaur (m)

d = 15.8*AU ; approximate distance between particle and sun (m)

deg = 33.77/!radeg ; angle where sun is positioned (rads)

year = 3.15576e7


rd = 100. ; Particle Radius


;; Solar pressure equation: Beta=Fr/Fg => this is a ratio of radiation pressure
;; force to gravitational force
;; Conditions for Beta
IF rd LE 0.2 THEN BEGIN
  B = (rd/0.1)*exp(1.-(rd/0.1))
ENDIF ELSE BEGIN
  B = 4./(exp(1)*(rd/0.1))
ENDELSE


;; EQUATIONS OF MOTION
f = fltarr(6)


f[0] = Y[3] ; x-component of velocity
f[1] = Y[4] ; y-component of velocity
f[2] = Y[5] ; z-component of velocity


; Particle's radial distance from central object
```

```
r = sqrt(Y[0]^2 + Y[1]^2 + Y[2]^2)

; If (r LT Rchar)THEN print, 'crash'


f[3] = -(G*M_centaur*Y[0])/r^3 + B*(G*M_sun*cos(deg))/d^2 ; Acceleration along
; x-axis
f[4] = -(G*M_centaur*Y[1])/r^3 ; Acceleration of particle along y-axis
f[5] = -(G*M_centaur*Y[2])/r^3 + B*(G*M_sun*sin(deg))/d^2 ; Acceleration along
; z-axis


Return, f


END


PRO PORBIT3D, revs, maxsteps, X, Y, time ;period ;


   ;+
   ; Description:
   ;     Simulates a particle's orbit using LSODE, a variable step-size integrator
   ; Params:
   ;     revs : number of revolutions particle takes
   ;     maxsteps : how many steps taken
   ;     X : time
   ;     Y : array [x,y,vx,vy] of stored positions and velocities of orbiting
   ;               particle
   ;     period/time : time range for simulation
   ; Uses:
   ;     Called by loop.pro
```

```
; Author: Juliet Pilewskie


;; PORBIT USES DESIGNATED TIME AND NUMBER OF STEPS TO FIND PERTURBED TRAJECTORY

;; OF PARTICLE ABOUT A CENTRAL BODY


; COMMON share, s_m

; COMMON test, rd


; CONSTANTS

M_sun = 1.9891e30 ; kg

M_centaur = 8.4e18 ; kg

G = 6.67e-11 ; m^3 kg^(-1) s^(-2)

AU = 1.49598e+11 ; m

Rchar = 1.24e5 ; Radius of centaur (m)

d = 15.8*AU ; approximate distance between particle and sun (m)

year = 3.15576e7


mult = 3.15 ; Number of Chariklo radii

s_m = mult*Rchar ; semi-major axis (m)


rd = 100. ; Particle Radius


; CONDITIONS FOR BETA

IF rd LE 0.2 THEN BEGIN

    B = (rd/0.1)*exp(1-(rd/0.1))

ENDIF ELSE BEGIN

    B = 4/(exp(1)*(rd/0.1))
```

ENDELSE

;; INITIAL CONDITIONS FOR ONE PARTICLE MASS

x0 = s_m ; x(t=0)

y0 = 0. ; y(0)

z0 = 0. ; z(0)

vx0 = 0. ; v_x(0)

vy0 = sqrt((G * M_centaur) / x0) ; v_y(0)

vz0 = 0. ; v_z(0)

time = (2*!pi*x0)/vy0 ; time it takes to complete one orbit
;print, time

Y = [x0,y0,z0,vx0,vy0,vz0] ; Vector of initial conditions

X = 0.0 ; Initialize time

;;DEFINING STEP SIZE

revs = 10.^8 ; Number of orbits around Chariklo

maxsteps = 10.^6 ; Maximum number of steps taken

H0 = (time*revs) / (maxsteps) ; Step−size

;print, H0

;H0 = (period*revs) / (maxsteps) ; Step−size

;; EMPTY ARRAYS FOR STORAGE

r1 = fltarr(maxsteps+1)

t = fltarr(maxsteps+1)

```
result = fltarr(6, maxsteps+1) ;  Empty 2D array for storing results


;; SOLVING DIFFERENTIAL EQUATION TO EXTRACT POSITIONS AND VELOCITIES OF

;; PARTICLE'S ORBIT AT VARIOUS RADIAL DISTANCES/PARTICLE RADII

H = H0

FOR n = 0, maxsteps DO BEGIN

      ; Numerical Integration

  result[*, n] = (y = LSODE(Y, X, H, 'FORCE3D', ATOL = 1e-6, RTOL = 1e-6))


  ; Storing Particle's Radial Distance

  r1[n] = sqrt(result[0,n]^2+result[1,n]^2+result[2,n]^2)


  ; MAKING SURE THAT INTEGRATION STOPS WHEN CHARIKLO CRASHES INTO CHARIKLO

  IF  r1[n] GE Rchar THEN BEGIN

    ;print, 'Step 1'

    X += H ; Updating time

    t[n] = X

    ;print, X

  ENDIF ELSE BEGIN

    t[n] = X + H

    BREAK

  ENDELSE


ENDFOR


  ; STORING RESULTS

  r2 = sqrt(result[0,*]^2+result[1,*]^2+result[2,*]^2)
```

```
idx = WHERE( r2 NE 0, nidx )

tidx = WHERE( t NE 0, ntidx )

IF nidx NE 0 THEN BEGIN

    xdir = result [0, idx ]

    ydir = result [1, idx ]

    zdir = result [2, idx ]

    vx = result [3, idx ]

    vy = result [4, idx ]

    vz = result [5, idx ]

ENDIF

IF ntidx NE 0 THEN BEGIN

    t = t [ tidx ]

ENDIF


; SAVING DATA
smstring = STRTRIM( mult, 2)
rstring = STRTRIM( rd, 2)
SAVE, FILENAME = 'r_'+smstring+'_3D.sav', t, xdir, ydir, zdir, vx, vy, vz


; PLOTTING ORBIT IN XY-PLANE
orbit = PLOT( xdir, ydir, ASPECT_RATIO = 1, TITLE = "Particle 's orbit, r=" +
rstring + '$\mu$m, D=' + smstring + '*Rchar', $
    XTITLE = "x-pos [m]", YTITLE = "y-pos [m]", ".");


;; KEPLER ELEMENTS
v_init = sqrt(vx0^2 + vy0^2 + vz0^2) ; Initial radial velocity
r_init = sqrt(x0^2 + y0^2 + z0^2) ; Initial position vector
```

```
r3 = sqrt(xdir^2+ydir^2+zdir^2) ; magnitude of position vector

v = sqrt(vx^2+vy^2+vz^2) ; magnitude of velocity vector

L = sqrt((ydir*vz − zdir*vy)^2+(xdir*vz − zdir*vx)^2 +(xdir*vy − ydir*vx)^2)

; magnitude of angular momentum vector


a0 = 1./((2./r_init)−(v_init^2/(G*M_centaur))) ; initial semimajor axis of

; orbit (m)

a = 1./((2./r2)−(v^2/(G*M_centaur))) ; semimajor axis of orbit (m)


e = (1.−L^2/(G*M_centaur*a))^(.5) ; eccentricity of orbit


Lz = xdir*vy − ydir*vx ; Angular momentum in z−direction

i = ACOS(Lz/L) ; inclination equation


Et = −((G/AU^3)*M_centaur)/(2*a) ; total orbital energy

E0 = −((G/AU^3)*M_centaur)/(2*a0) ; initial orbital energy

energy = PLOT(t/year, Et/E0, XTITLE = "time [yr]", THICK = 2, Name = 'E over

E0', TITLE = 'Change in Total Energy, R/R0 ='+STRTRIM(STRING(smstring,

Format='(F5.2)'),1))


; Equation for initial angular momentum

J0 = M_centaur * (sqrt(((y0/AU)*(vz0/AU) − (z0/AU)*(vy0/AU))^2 + ((x0/AU)*

(vz0/AU) − (z0/AU)*(vx0/AU))^2 + $

  ((x0/AU)*(vy0/AU) − (y0/AU)*(vx0/AU))^2)) ;


; Angular momentum equation

J = M_centaur * (sqrt(((ydir/AU)*(vz/AU) − (zdir/AU)*(vy/AU))^2 + ((xdir/AU)*
```

```
( vz/AU) − ( zdir/AU)∗(vx/AU))^2 + (( xdir/AU) ∗ (vy/AU) − ( ydir/AU) ∗
( vx/AU))^2))


; Angular momentum and energy plot
;Jz0 = M_centaur ∗((x0/AU)∗(vy0/AU) − (y0/AU)∗(vx0/AU))
;Jz = M_centaur ∗((xdir/AU)∗(vy/AU) − (ydir/AU)∗(vx/AU))
ang_mom = PLOT( t/year , J/J0 , XTITLE = "time [ yr ]" , 'g' , NAME = 'J over J0',
THICK = 3, /OVERPLOT) ; , /ynozero , chars=2
;ang_mom_z = PLOT( t/year , Jz/Jz0 , 'g' , XTITLE = "time [ yr ]", NAME = 'Jz over
Jz0', THICK = 3,/OVERPLOT)
leg = LEGEND( Target=[ang_mom , energy ] )


;; ANALYTICAL RESULTS (FOR 2D Model only )
;    e_max = 1. − ( Rchar/s_m) ; Maximum eccentricity
;
;    h_m = (G∗M_centaur∗s_m )^(.5) ; Specific ( per unit mass) angular momentum
;    f = B∗(G∗M_sun)/d^2 ; Specific acceleration due to solar radiation pressure
;    lam = (1.5∗h_m∗f )/(G∗M_centaur) ; Equals de/dt
;
;    t2 = e_max/lam
;
;    t_life = [0. , e_max/lam] ; Lifetime of particle (s)
;    e_m = [0. , e_max] ; for plotting e_max


;; ANALYZING ORBIT BY MEANS OF KEPLERIAN ELEMENTS


; Orbital inclination plot
```

```
inc = PLOT(t/year, i, Xtitle = "t (yr)", Ytitle = "i (rads)", Title =
"Orbital inclination over time") ; semi−major axis plot


; Semi−Major Plot
semi = PLOT(t/year, a/a0, Xtitle = "t (yr)", Ytitle = "a/a0", Title =
"Semi−major axis over time") ; semi−major axis plot
e1 = PLOT(t/year, e, Xtitle = "t (yr)", Ytitle = "e", Title = 'Eccentricity
over time, r=' + STRTRIM(STRING(rstring,Format='(F5.1)'),1) + '$\mu$m, R/R0='
+ STRTRIM(STRING(smstring, Format='(F5.2)'),1), Name = 'Numerical') ;
eccentricity found numerically
;e2 = PLOT(t_life/year, e_m, /OVERPLOT, 'g', Name = 'Analytical') ;
eccentricity found analytically
;leg = LEGEND(Target=[e1,e2])


;; PERICENTER/APOCENTER PLOT
r_apo = s_m*(1+e)
r_peri = s_m*(1−e)
Rlist = make_array(N_elements(t),value=Rchar)
rplot1 = PLOT(t/year, r_apo/Rchar, Xtitle = "t (yr)", Ytitle = "r/R0", Title
= '3D Pericenter and Chariklo radius, R/R0=' + STRTRIM(STRING(smstring,
Format='(F5.2)'),1), 'b:', Name = 'Apocenter')
rplot2 = PLOT(t/year, r_peri/Rchar,'gD', Name = 'Pericenter', /OVERPLOT)
rplot3 = PLOT(t/year, Rlist/Rchar, Name = 'Radius of Chariklo', /OVERPLOT)
leg = LEGEND(Target=[rplot1,rplot2,rplot3], /DEVICE, Position = [287,413])


END
```